# Determination of the asymptotic $D$- to $S$-state ratio for $^6$Li via $(^6\vec{\text{Li}},d)$ transfer reactions

K. D. Veal,[1,2,*] C. R. Brune,[1,2] W. H. Geist,[1,2,*] H. J. Karwowski,[1,2] E. J. Ludwig,[1,2] E. E. Bartosz,[3] P. D. Cathers,[3] T. L. Drummer,[3,†] K. W. Kemper,[3] A. M. Eiró,[4] F. D. Santos,[4] B. Kozlowska,[2,5] H. J. Maier,[6] and I. J. Thompson[7]

[1]*Department of Physics and Astronomy, University of North Carolina at Chapel Hill, Chapel Hill, North Carolina 27599-3255*

[2]*Triangle Universities Nuclear Laboratory, Durham, North Carolina 27788-0308*

[3]*Department of Physics, Florida State University, Tallahassee, Florida 32306-4350*

[4]*Departamento de Fisica and Centro de Fisica Nuclear da Universidade de Lisboa, Lisboa, Portugal*

[5]*Institute of Physics, University of Silesia, Katowice, Poland*

[6]*University of Munich, Garching, Germany*

[7]*Department of Physics, University of Surrey, Guildford GU2 5XH, United Kingdom*

(Received 19 July 1999; published 16 November 1999)

Measurements of cross section, vector analyzing power $A_y$, and tensor analyzing powers $A_{zz}$ and $A_{xz}$ over the angular range $10° \leqslant \theta_{\text{lab}} \leqslant 40°$ have been performed at $E(^6\text{Li}) = 34$ MeV for the $^{58}\text{Ni}(^6\vec{\text{Li}},d)^{62}\text{Zn}$ and $^{40}\text{Ca}(^6\vec{\text{Li}},d)^{44}\text{Ti}$ reactions leading to the ground state and first excited state of both residual nuclei. The reactions are described by distorted-wave Born approximation calculations, assuming a direct $\alpha$-particle transfer mechanism. The asymptotic $D/S$ state ratio $\eta$ for the $d+\alpha$ relative wave function in $^6$Li is determined. In this one-step analysis, the best fit to the tensor observables leads to a value of $\eta = +0.0003 \pm 0.0009$. This value is in disagreement with most of the previous theoretical and empirical determinations of $\eta$. An investigation of two-step reaction mechanisms is performed, allowing the $J^\pi = 3^+$, $2^+$, and $1^+$ states in $^6$Li to contribute to the transfer reaction channel. Reasonable agreement is achieved with the cross section and vector analyzing power data for several possible two-step amplitudes. It is found that the fitted magnitude of $\eta$ increases with increasing two-step amplitude, giving $\eta = -0.0030 \pm 0.0022$ for unit amplitude, therefore not changing significantly from our one-step result. [S0556-2813(99)00812-2]

PACS number(s): 21.45.+v, 24.70.+s, 25.70.Hi, 24.50.+g

## I. INTRODUCTION

One manifestation of the nucleon-nucleon tensor force is the presence of nonspherical or deformed components in the ground-state wave functions of light nuclei. A measure of these nuclear deformations is the ratio of the $D$- and $S$-state asymptotic normalization constants $\eta$ [1]. A $D$-state component in the wave function of a nucleus is manifested directly by a nonzero $D$- to $S$-state ratio and/or by a nonzero quadrupole moment. In the case of the deuteron a $D$ state is predicted directly on the basis of the nonzero quadrupole moment. The value of $\eta$ for the deuteron $\eta(d)$ has been measured by sub-Coulomb $(\vec{d},p)$ reactions [2] to be $+0.0256 \pm 0.0004$ and is in very good agreement with theoretical calculations [3]. For the $A=3$ systems a $D$ state can also exist between the deuteron and the neutron (proton) in the triton ($^3$He). Values of $\eta(t) = -0.0411 \pm 0.0013 \pm 0.0012$ [4] and $\eta(^3\text{He}) = -0.0386 \pm 0.0045 \pm 0.0011$ [5], for example, have been measured by $(\vec{d},t)$ and $(\vec{d},{}^3\text{He})$ reactions near or below the Coulomb barrier, where the first error reported is statistical and the second is systematic. These values agree well with theoretical predictions based on solutions of Faddeev-type equations [6,7] and with recent variational calculations [8]. Even the $d+d$ configuration of the $\alpha$ particle, which has $J^\pi = 0^+$, has a $D$-state component in its wave function [9,10]. Though generally parametrized in terms of the DWBA parameter $D_2$ and not $\eta(^4\text{He})$, the $D$ state in the $d+d$ configuration has been established to within about 20%. Reviews of the status of the studies of $D$ states in light nuclei (through 1990) are given in Refs. [1,3,11].

In principle, $^6$Li can also contain a $D$ state in its ground-state wave function. Cluster configurations of $d+\alpha$ or $t+{}^3\text{He}$ can have either $l=0$ or 2 units of relative orbital angular momentum and still maintain $J^\pi = 1^+$ for the $^6$Li ground state. The $d+\alpha$ configuration is expected to be much larger based on the large binding energy of the $\alpha$ particle and the small separation energy between the $\alpha$ particle and the deuteron (1.47 MeV). This is further supported by breakup and knockout reactions on $^6$Li [12,13], where the $d+\alpha$ probability in the ground state of $^6$Li obtained from $^6\text{Li}(e,e'd)^4\text{He}$ knockout reactions is 0.73. Therefore, most of the theoretical and experimental investigations into the $^6$Li $D$ state have focused on the $d+\alpha$ configuration. However, contrary to the lighter nuclei, the asymptotic $D$- to $S$-state ratio for the $d+\alpha$ relative motion in $^6$Li, denoted here simply as $\eta$, is not well determined.

Knowledge of the $D$-state properties in $^6$Li is important for probing the tensor force between the deuteron and $\alpha$ cluster as well as providing information about the wave functions of the valence $p$-shell nucleons. A practical application of this information is the determination of the neutron polarization when $^6$Li is used as a polarized neutron target [14]. The presence of a $D$ state in the ground-state wave function

*Present adddress: Los Alamos National Laboratory, Los Alamos, NM 87545.

†Present address: University of Illinois, Urbana, IL 61800.

 

of $^6$Li would tend to dilute the neutron polarization since, in this state, the deuteron spin would be antiparallel to the spin of the $^6$Li, an orientation opposite to that for the particles in the predominant $S$ state.

In the present paper we report on a determination of $\eta$ from the analysis of tensor analyzing powers (TAPs) from $(\vec{^6\mathrm{Li}},d)$ transfer reactions. This analysis is based on the fact that the magnitude and sign of the calculated TAPs are proportional to $\eta$. In Sec. II we present an overview of the previous determinations of $\eta$ highlighting the theoretical and experimental discrepancies. In Sec. III we describe the experimental procedure. In Sec. IV the $\alpha$-transfer analysis is performed, including direct one-step $\alpha$-transfer DWBA calculations in Sec. IV A, and the determination of $\eta$ from the TAP data, with a discussion of uncertainties involved, is in Sec. IV B. Furthermore, in Sec. V we investigate the effects of two-step mechanisms in $(^6\mathrm{Li},d)$ reactions on our determination of $\eta$. Finally, in Sec. VI we compare our results with previous analyses and discuss the resulting implications. Many of these results have been reported in a recent Letter [15] and additional information may be obtained in Ref. [16].

## II. BACKGROUND

In the $^6$Li nucleus the radial $d+\alpha$ wave function $u_l(r)$ with relative orbital angular momentum $l$ behaves asymptotically as [1]

$$\lim_{r\to\infty} b_l\, u_l(r) \to \frac{N_l}{\beta r} W_{-\xi,l+(1/2)}(2\beta r). \tag{1}$$

Here $r$ is the separation distance between the $\alpha$ and the deuteron, $W_{-\xi,l+(1/2)}$ is a Whittaker function involving the Coulomb parameter $\xi$, $N_l$ is an asymptotic normalization constant, and $\beta$ is the wave number at the $^6\mathrm{Li}\to d+\alpha$ vertex. The asymptotic $D$- to $S$-state ratio is defined as $\eta = N_2/N_0$. The $b_l$'s are the spectroscopic amplitudes of the $l$th partial wave functions and are normalized such that $b_0^2 + b_2^2 = 1$. We note that although the spectroscopic factor for the $d+\alpha$ configuration is smaller than 1 (see, for example, Ref. [17]), this quantity will cancel in the ratio $N_2/N_0$ and therefore will not affect the determination of $\eta$.

At present, the only unambiguous evidence for the existence of a $D$ state in $^6$Li is the nonzero electric quadrupole moment $Q = -0.083$ fm$^2$ [18], implying the $^6$Li nucleus has a slightly oblate shape. Nishioka *et al.* [19] suggested that in a $d+\alpha$ cluster model $Q$ could originate from a subtle cancellation of the deuteron quadrupole moment ($Q_d = +0.2859$ fm$^2$) and a term which arises from the $D$ state in the $d+\alpha$ relative wave function. By admixing an appropriate amount of $D$ state into the wave function, they were able to reproduce the $^6$Li quadrupole moment. This resulted in $\eta = -0.0112$ (not the $\eta = -0.014$ quoted in Ref. [1]). It should be pointed out that the work of Nishioka *et al.* used an older slightly smaller value for $Q$ than that of Ref. [18]. In the $d+\alpha$ cluster model of Ref. [19], the value of $\eta$ corresponding to $Q$ of Ref. [18] is $-0.0127$ [20].

Three-body models ($\alpha+n+p$) have generated predictions of $\eta$ ranging from $+0.0055$ to $+0.0194$ [3] depending on the form of the $NN$ and $\alpha N$ potential assumed in the calculation. Predictions from these models are in excellent agreement with properties of $^6$Li such as the charge form factors, the charge and matter radii, and the magnetic moment but, in each case, fail to reproduce the negative quadrupole moment. There seems to be a systematic difficulty in the three-body models in that they all predict $Q>0$ [3,14,21]. Furthermore, though a numerical value was not reported, the three-body model of Ref. [21] predicted $\eta>0$.

An alternative method for modeling $^6$Li is the ''no-core shell model'' [22] that has recently been used with a large basis, and with different renormalized effective interactions based on the Reid 93 nucleon-nucleon potential. This calculation reproduces well the level spectrum of $^6$Li, and predicts a quadrupole moment for the ground state of $Q = -0.052$ fm$^2$, the closest to the experimental value of any theoretical prediction that we are aware of.

Perhaps the most sophisticated microscopic calculations to date are those of the Illinois group using the Green's function Monte Carlo technique to calculate properties of the ground and excited states in $A\leqslant 7$ nuclei [23,24]. Using a variational Monte Carlo (VMC) technique, this group calculated wave functions and binding energies for nuclei through $A=6$ [25]. They calculated the $d+\alpha$ configuration in the $^6$Li wave function, leading to density distributions and normalization constants that in the $S$-wave case are close to experimental values. However, the $D$-wave component does not reproduce the $D$-state observables, predicting a value for the quadrupole moment of $Q = -0.8 \pm 0.2$ fm$^2$, one order of magnitude larger than the experimental value [18], and a value of $\eta = -0.07 \pm 0.02$ for the $\langle d\alpha | ^6\mathrm{Li}\rangle$ bound-state overlap. It has been pointed out [24,25] that the long-range part of the wave functions are not well determined by the Monte Carlo technique so their estimates for $\eta$ are perhaps not very reliable. However, their estimates of the asymptotic $D/S$ ratios for the lighter nuclei are in good agreement with experiment. A more recent calculation [26] of the same type that should be closer to convergence for $A=6$ nuclei results in smaller values of $Q = -0.33 \pm 0.18$ fm$^2$ and $\eta = -0.03$.

Experimentally the situation is similar, in that there is no consensus as to the magnitude or sign of $\eta$. One of the first investigations was a forward dispersion relation analysis of $d-\alpha$ scattering [27]. In that analysis, the residues of the scattering pole, which correspond to the virtual formation and decay of a $^6$Li nucleus, can be related to the $S$ and $D$ asymptotic normalization constants. Three residues were determined via extrapolation to the pole energy, from which the asymptotic normalization constants were determined. The ratio of the $D$- and $S$-state constants results in $\eta = +0.005 \pm 0.014$.

The two-body model of Nishioka *et al.* [19] was applied to $\vec{^6\mathrm{Li}} + ^{58}\mathrm{Ni}$ scattering at $E_{\mathrm{c.m.}} = 18.1$ MeV. They assumed that a $D$ state in the $d+\alpha$ wave function with $\eta = -0.0112$ was responsible for generating the observed positive ${}^T T_{20}$ ($= A_{yy}/\sqrt{2}$) data. In this analysis, the ground state of the $^6$Li was also assumed to be coupled to the $T=0$ excited

states ($3^+$ 2.19 MeV, $2^+$ 4.31 MeV, $1^+$ 5.65 MeV) and the polarization observable was approximately reproduced.

The same elastic scattering process was measured by Dee *et al.* [20] at $E(^6\mathrm{Li})=70.5$ MeV and analyzed using coupled channel calculations with potentials generated by a cluster folding method. An $\alpha+d$ configuration of $^6$Li was assumed to be represented by a Woods-Saxon geometry ($R=1.9$ fm, $a=0.65$ fm) and was used to describe three excited *D*-wave resonances, within the weak binding approximation. The $^{T}T_{20}$ data were generally well described when the strength of the *D*-state component of the bound-state wave function used led to a value of $\eta=-0.0127$. However the results for the other observables like $T_{20}$ $(=A_{zz}/\sqrt{2})$ and $iT_{11}$ $(=\sqrt{3}A_y/2)$, for which the agreement was not so good, were much less conclusive about either the sign or the magnitude of $\eta$. The data of Ref. [20] were reanalyzed by Rusek *et al.* [28] assuming a larger channel coupling mechanism including nonresonant continuum breakup effects on the elastic scattering data. From an analysis of the $^{T}T_{20}$ data it was suggested that $\eta$ should be about half that of Dee *et al.*, or $\eta\approx-0.0064$, but the $T_{20}$ predictions did not show much sensitivity to the magnitude or sign of $\eta$. Again, as with the previous analysis, the vector analyzing power (VAP) data were not well described by the calculations.

Punjabi *et al.* [29] detected deuterons and $\alpha$ particles from the breakup of polarized $^6$Li on $^1$H at 4.5 GeV. Viewed within the plane-wave impulse approximation, $T_{20}$ is sensitive to interference effects between the *S*- and *D*-state components of the $^6$Li wave function. A plot of $T_{20}$ versus the transferred momentum $q$ showed that for the three-body models of Ref. [3] with $\eta>0$, $T_{20}$ should be positive for large $q$ and negative for small $q$ with the sign change occurring at about $q=0.12$ GeV/$c$. Data from the detected deuterons and $\alpha$ particles qualitatively resembled this trend, from which it was concluded that $\eta$ should be positive.

Santos *et al.* [30] analyzed the TAPs from the $^6\mathrm{Li}(\vec{d},\alpha)^4\mathrm{He}$ reaction at 10 MeV. Assuming the reaction proceeded via a direct transfer mechanism, it was argued that the best agreement with the TAP data was achieved when the *D* state of $^6$Li and $^4$He had the same sign. Thus since the $D/S$ ratio for $^4$He is negative, it was concluded that $\eta$ for $^6$Li should also be negative, with a magnitude in the range $-0.015<\eta<-0.010$.

Kukulin *et al.* [31] have calculated the $d+^4$He tensor interaction from an inversion of $d-\alpha$ phase shifts. Fitting the $^3S_1$ and $^3D_1$ low-energy phase shifts, the binding energy, and $Q$, they determine two $d+^4$He tensor interactions, from which $\eta$ is calculated to be $-0.0115$ or $-0.0120$.

Recently, George and Knutson [32] have performed a phase shift analysis of $^6\vec{\mathrm{Li}}+^4$He scattering at $E_{\mathrm{c.m.}}=2.2$ MeV. In their analysis, the lower partial waves were fitted whereas the higher partial waves ($l\geq4$) were determined from Coulomb-wave Born approximation calculations for deuteron exchange. With several phase shift and mixing parameters being sensitive to the asymptotic constants, they found $\eta=-0.026\pm0.006\pm0.010$.

The results for $\eta$ obtained by the various groups are presented in Fig. 1. We see that, even neglecting the VMC

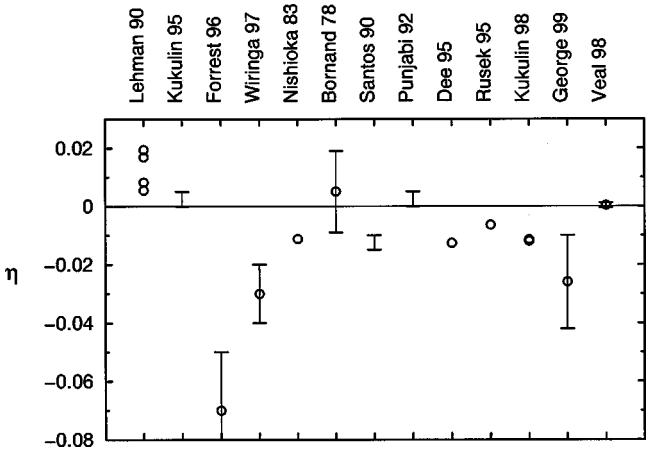


FIG. 1. Summary of previous theoretical and experimental determinations of $\eta$ for $^6$Li. See the text for a detailed discussion of each result.

results that almost certainly overpredict the magnitude of the *D*-state as discussed by Eiró and Thompson [33], there is considerable disagreement between the different determinations, showing the need for further investigations. It is important to note that some of these results were reported without establishing errors or reported only the sign of $\eta$ but not the magnitude, while others were obtained from many observables involving a systematic study of uncertainties. Therefore these results are not equally important and should not be considered with equal weight.

In the present work we determine $\eta$ for the $d+\alpha$ relative motion in $^6$Li by an analysis of the TAPs from $(^6\vec{\mathrm{Li}},d)$ transfer reactions. We use the fact that DWBA calculations of the TAPs from these reactions scale with the magnitude and sign of $\eta$, as discussed in Sec. IV. This method has been applied successfully in studies of the *D* state in the $A=2-4$ nuclei for the TAPs from deuteron-induced transfer reactions [2,4,5,34].

We have measured the TAPs $A_{zz}$ and $A_{xz}$ for the $^{58}\mathrm{Ni}(^6\vec{\mathrm{Li}},d)^{62}\mathrm{Zn}$ and the $^{40}\mathrm{Ca}(^6\vec{\mathrm{Li}},d)^{44}\mathrm{Ti}$ reactions at $E(^6\mathrm{Li})=34$ MeV leading to the $0^+$ ground and $2^+$ first-excited state for each reaction. We measured the VAP $A_y$ for each transition to assist in modeling the reaction mechanism. Furthermore, we have also measured cross section and VAP for $^6\vec{\mathrm{Li}}+^{58}$Ni scattering, also at 34 MeV, in order to optimize the optical potential parameters. The particular $(^6\mathrm{Li},d)$ reactions measured here were chosen to satisfy a number of criteria. The $^{58}$Ni and $^{40}$Ca targets were chosen because they have a reasonable $(^6\mathrm{Li},d)$ cross section ($\gtrsim10$ $\mu$b/sr) for the g.s. transitions, can be made fairly thick ($\sim1$ mg/cm$^2$) to maximize the count rate, they lead to a daughter nucleus with well-separated ($\sim1$ MeV) low-lying states, and they proceed through unique angular momentum transfers.

We use the distorted-wave Born approximation (DWBA) to model the reactions assuming a direct $\alpha$-particle transfer mechanism. As will be discussed in Sec. IV A, we have achieved good agreement with the data in describing the reactions by a one-step mechanism. However, in view of evidence that the analyzing powers from $(\vec{d},^6\mathrm{Li})$ reactions at

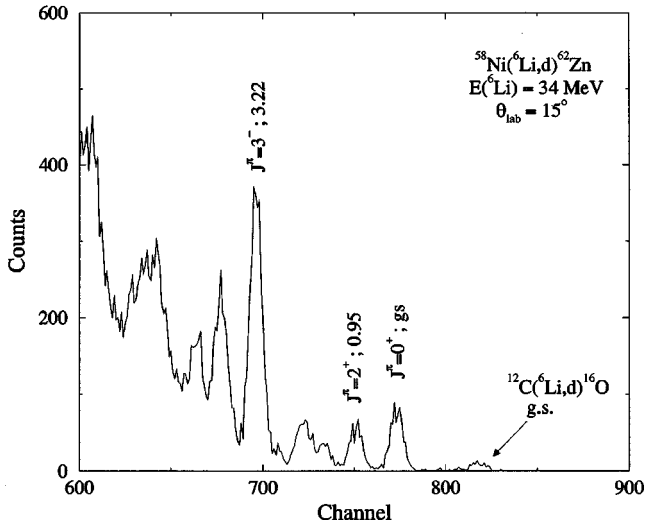


FIG. 2. Sample spectrum for the $^{58}$Ni($^{6}\vec{\text{Li}},d$)$^{62}$Zn reaction at $E(^{6}\text{Li})=34$ MeV. Excitation energies are given in MeV.

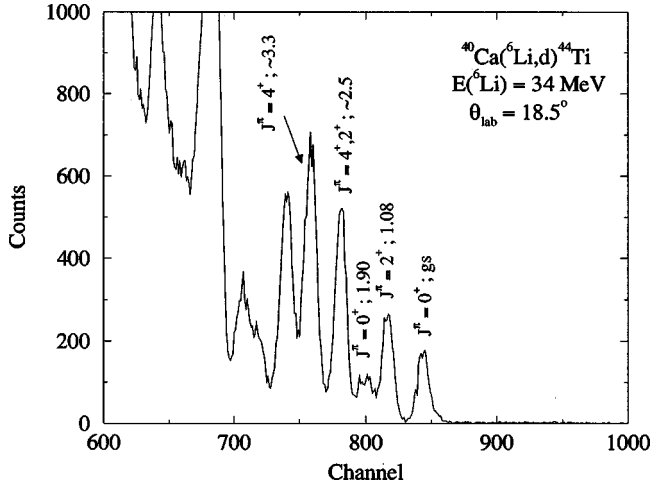


FIG. 3. Sample spectrum for the $^{40}$Ca($^{6}\vec{\text{Li}},d$)$^{44}$Ti reaction at $E(^{6}\text{Li})=34$ MeV. Excitation energies are given in MeV.

lower interaction energies [35] proceed via a two-step mechanism through excited states of $^{6}$Li, we also include an investigation of two-step mechanisms in the analysis of the present ($^{6}\vec{\text{Li}},d$) reactions (Sec. V).

### III. DESCRIPTION OF THE EXPERIMENTS

The experiments were performed at Florida State University using the optically pumped polarized lithium ion source [36]. The polarization state of the beam was changed in the source every two to three minutes between an unpolarized state and a state with either large vector or large tensor polarization. The orientation of spin direction of the beam particles for measuring the different analyzing powers was controlled by the use of a Wien filter.

The $^{6}\vec{\text{Li}}$ ions were accelerated to 34 MeV with the Super FN Tandem accelerator into an 85-cm-diameter scattering chamber. Two pairs of Si $\Delta E$-$E$ detector telescopes separated by 15° were placed on rotating platforms on each side of the beam. The telescopes, consisting of between 4 to 6 mm of Si with 1- or 2-mm Si $\Delta E$ detectors, were positioned 14.6 cm from the target. The $A_y$ and $A_{zz}$ data for the $^{58}$Ni($^{6}\vec{\text{Li}},d$)$^{62}$Zn reaction were taken with telescopes having an angular acceptance of $\pm 2.2°$ and subtending a solid angle of 4.7 msr while the $A_{xz}$ data for the $^{58}$Ni($^{6}\vec{\text{Li}},d$)$^{62}$Zn reaction and all of the data for the $^{40}$Ca($^{6}\vec{\text{Li}},d$)$^{44}$Ti reaction were taken with telescopes having an angular acceptance of $\pm 2.0°$ and solid angle of 6.2 msr. A 0.08-mm thick Ta foil was placed in front of each telescope to stop the elastically scattered $^{6}$Li ions. The ground- and first-excited state transitions for both reactions were well resolved, except for a few instances where the presence of $^{12}$C build up on the target prevented the extraction of the yields. Sample deuteron spectra are shown in Figs. 2 and 3. Furthermore, a small Si detector was placed at 135° with respect to the incident beam direction to monitor the target and to normalize yields for relative cross-section measurements.

The $^{58}$Ni targets (>99.76% enriched) were self-supporting rolled foils ranging in thickness from 0.8 to 2.0 mg/cm$^2$. The $^{40}$Ca targets consisted of 0.9 mg/cm$^2$ of natural Ca sandwiched between 0.3-mg/cm$^2$ layers of Au.

After passing through the target the beam entered a secondary scattering chamber where the polarization was monitored via $^{4}$He($^{6}\vec{\text{Li}},^{4}$He)$^{6}$Li scattering, as described in Refs. [37,38]. Typical beam polarizations on target were $p_z \approx -0.6$ and $p_{zz} \approx -1.1$.

The analyzing powers were determined by forming the asymmetry relations

$$A_{zz}=\frac{L+R-2}{p_{zz}}, \tag{2}$$

$$A_{xz}=\frac{L-R}{p_{zz}}, \tag{3}$$

and

$$A_y=\frac{L-R}{3p_z}, \tag{4}$$

where $L$ ($R$) is the ratio of the counts collected in the left (right) detector in the polarized state divided by the counts collected in the unpolarized state normalized by the charge collected and computer dead time during data taking in each state. The TAP $A_{zz}$ was determined when the spin quantization axis was pointed along the incident beam direction, $A_{xz}$ was determined when the axis was pointed 45° from the incident beam direction, but in the scattering plane, and $A_y$ was measured when the spin axis was perpendicular to the scattering plane.

In order to assist us in our direct transfer calculations, it was necessary to measure $^{6}\vec{\text{Li}}+^{58}$Ni scattering also at 34 MeV. These data were measured with a 200 $\mu$g/cm$^2$ $^{58}$Ni target using techniques similar to those described in Ref. [39]. The ratios of the observed cross section to the Ruther-

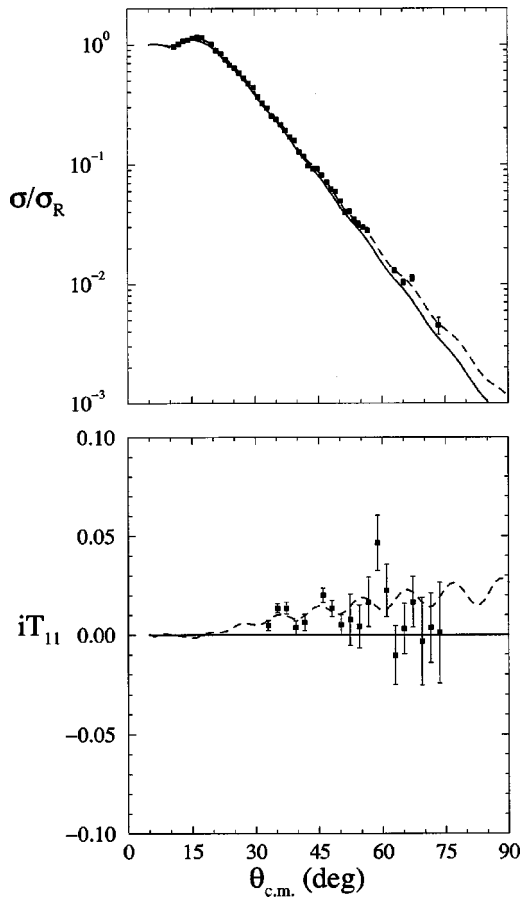


FIG. 4. Angular distributions of the cross section (as ratio to Rutherford scattering) and VAP for $^{6}\vec{\mathrm{Li}}+^{58}\mathrm{Ni}$ elastic scattering at $E(^{6}\mathrm{Li})=34$ MeV. The solid curve is an OM calculation using the global parametrization of Cook [43] while the dashed curve uses the OM parameters given in Table I.

ford cross section $\sigma/\sigma_R$ and the VAP $iT_{11}$ are shown in Fig. 4. The cross section drops by $\sim 3$ orders of magnitude below that for Rutherford scattering by $\theta_{\mathrm{c.m.}}\approx 90°$. The VAP is small (typically $<0.02$) and positive. These data, though smaller in magnitude, resemble VAP data taken at lower energies [19]. For completeness, in Fig. 5 we show previously measured elastic scattering data for $^{6}\mathrm{Li}+^{40}\mathrm{Ca}$, also at 34 MeV [40].

Relative cross sections were measured for the $^{58}\mathrm{Ni}(^{6}\vec{\mathrm{Li}},d)^{62}\mathrm{Zn}$ reaction by taking the ratio of the counts during the unpolarized-beam runs in the chamber detectors with the counts in a gate set in the breakup spectrum in the fixed-angle monitor detector. The relative yields were normalized at forward angles to the cross section data of Ref. [41]. Cross sections were not extracted for the $^{40}\mathrm{Ca}(^{6}\vec{\mathrm{Li}},d)^{44}\mathrm{Ti}$ reaction because the Au backings of the Ca targets contributed to the breakup spectrum in the monitor detector. Since the exact ratio of Ca to Au for each target was not known we have used 32 MeV cross section data [42] for the $^{40}\mathrm{Ca}(^{6}\mathrm{Li},d)^{44}\mathrm{Ti}$ reaction in addition to the present 34 MeV analyzing power data to assist in establishing the reaction mechanism.

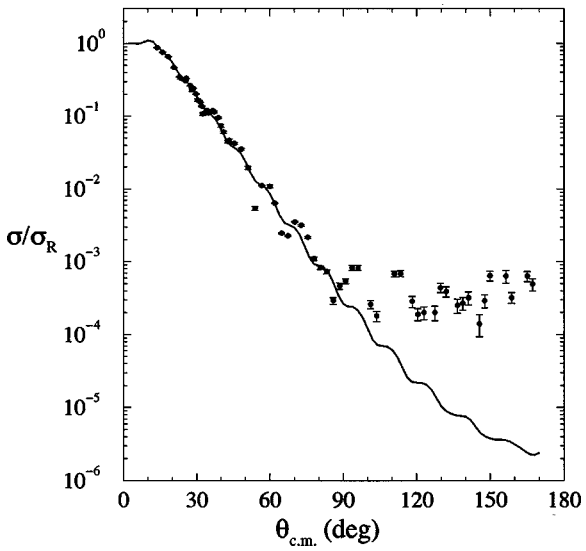


FIG. 5. Angular distribution of the cross section (as ratio to Rutherford scattering) for $^{6}\mathrm{Li}+^{40}\mathrm{Ca}$ scattering at $E(^{6}\mathrm{Li})=34$ MeV. The data are from Ref. [40]. The solid curve is the result of an OM calculation using the parametrization of Cook [43] as given in Table I.

The cross section, VAP, and TAPs for the the $(^{6}\vec{\mathrm{Li}},d)$ transfer reaction data are shown in Figs. 6–10. The cross sections are small (of the order $\sim 10$ $\mu$b/sr for the $0^+$ transitions and $\sim 30$ $\mu$b/sr for the $2^+$ transitions) and oscillatory. The VAPs are generally large and oscillatory while the

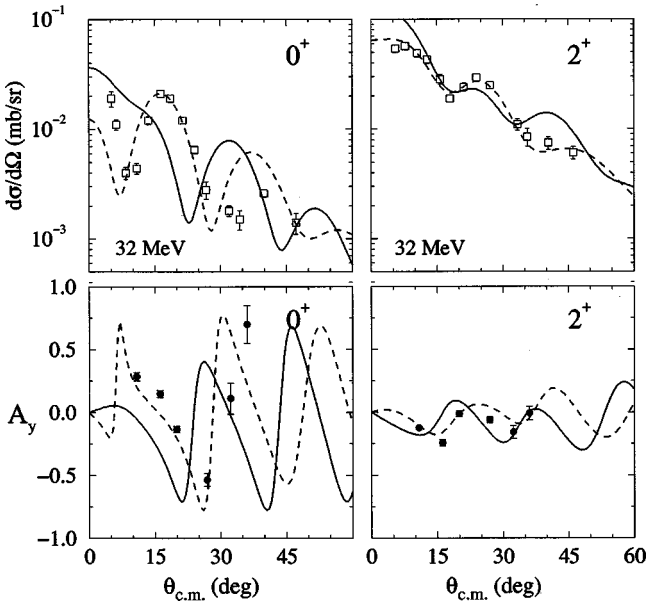


FIG. 6. Angular distributions of $d\sigma/d\Omega$ (32 MeV) and $A_y$ (34 MeV) for the $^{40}\mathrm{Ca}(^{6}\vec{\mathrm{Li}},d)^{44}\mathrm{Ti}$ reaction leading to the $0^+$ g.s. and the $2^+$ first excited state. The open squares (□) are from Ref. [42] while the closed circles (●) are the present data. The solid curves are the results of finite-range DWBA calculations using the initial global parameters. The dashed curves correspond to calculations with the deuteron OM radius parameter $r_0$ decreased by 12%. The calculations of $d\sigma/d\Omega$ are normalized to the data.

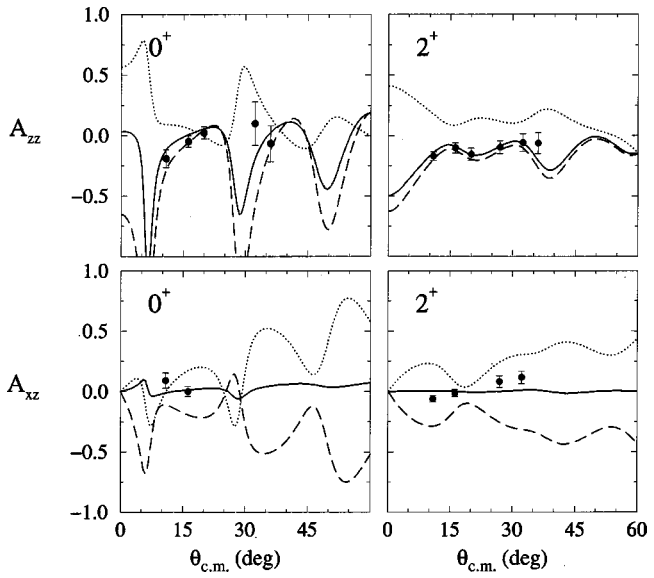


FIG. 7. Angular distributions of $A_{zz}$ and $A_{xz}$ for the $^{40}$Ca($^{6}\vec{\text{Li}}$,$d$)$^{44}$Ti reaction at $E(^6\text{Li})=34$ MeV. The solid curves assume a value of $\eta$ that results in the best fit to that analyzing power (see Table II). The dashed (dotted) curves correspond to calculations with $\eta=+0.015$ $(-0.015)$.

TAPs are much smaller (typically $\lesssim 0.1$) and mostly negative. The error bars shown are statistical only.

## IV. DIRECT TRANSFER ANALYSIS

### A. DWBA calculations

Since the targets used here have $J^\pi=0^+$, the observed transitions are populated with a unique angular momentum transfer: $l=0$ to the $0^+$ ground states and $l=2$ to the $2^+$ first-excited states. To perform the direct-transfer calculations we must first describe entrance and exit channel distorted waves and the wave functions for the two bound states in the reaction. The distorted waves are determined from $^6$Li and deuteron scattering calculations. The bound-state wave functions describe the overlaps of $^6$Li with $d+\alpha$ for the entrance channel and $^{62}$Zn with $^{58}$Ni$+\alpha$ or $^{44}$Ti with $^{40}$Ca $+\alpha$ for the exit channel.

The first step in the DWBA calculations of the ($^6$Li,$d$) reactions was the selection of suitable optical model (OM) parameters to calculate the distorted waves. The optical model potential is assumed to have the form

$$U_{OMP}(r)=-V_0 f(r,r_0,a_0) - i\left[W_i f(r,r_i,a_i)-4a_D W_D \frac{d}{dr} f(r,r_D,a_D)\right] + V_{LS}\left(\frac{\hbar}{m_\pi c}\right)^2 (\vec{L}\cdot\vec{S})\frac{1}{r}\frac{d}{dr} f(r,r_{LS},a_{LS}) + V_c(r), \tag{5}$$

where $f(r,r_x,a_x)$ has the usual Woods-Saxon form

$$f(r,r_x,a_x)=\frac{1}{1+\exp[(r-r_x A^{1/3})/a_x]}, \tag{6}$$

and $V_c$ is taken to be the Coulomb potential of a uniformly charged sphere with radius $R_c=r_c A^{1/3}$.

Cook [43] performed a global parametrization of $^6$Li scattering by making simultaneous fits to 44 $^6$Li scattering data sets covering a wide range of targets and energies assuming that the OM potential had only real and volume imaginary terms. From the upper panel of Fig. 4 it can been seen that OM calculations using the global parameters of Cook [43], shown as the solid curve, underpredict the cross section for $^6$Li$+^{58}$Ni scattering. To improve the agreement between the data and the calculations, we performed a search on the OM potential parameters with the computer code HERMES [44] using the parameters of Ref. [43] as the starting values. The results of this search are given in Table I and the OM calculation using these parameters are shown as the dashed curves in Fig. 4. The largest changes in the parameters with respect to those of Ref. [43] are in the imaginary potential where a 10% decrease in the depth and a 16% decrease in the diffuseness were needed to fit the scattering data. The agreement between the OM calculations and the $^6$Li$+^{40}$Ca data shown in Fig. 5 is not quite as good as for the $^{58}$Ni data mostly due to the large angle data which does not fall off as predicted by the OM. Attempts to fit these data within the framework of the OM have generally been unsuccessful [43,40]. As the more forward angle data ($\lesssim 60°$) are still well described, no changes were made in the parameters of the central part from that of Cook [43]. These parameters are also summarized in Table I.

A spin-orbit potential was added in order to fit the elastic VAP data. The parameters which resulted in the best fit are given in Table I and a calculation using these parameters is shown as the dashed curve in the lower panel of Fig. 4. The calculation agrees well with the more forward angle data whereas it appears to become out of phase with the data at $\theta_{\text{c.m.}}\approx 55°$. Including the spin-orbit term in the OM potential did not change the predicted elastic scattering cross section, in agreement with the conclusion of Chua *et al.* [45]. These spin-orbit parameters were also used in the $^6$Li$+^{40}$Ca calculations.

The exit channel parameters describing the deuteron scattering distorted waves were taken from the potential set *L* of Daehnick, Childs, and Vrcelj [46], which we will denote as DCV. This parametrization contains a real volume, imaginary surface, imaginary volume, and spin-orbit potential. Of course, there is no data describing $d+^{62}$Zn or $d+^{44}$Ti scattering as these nuclei are radioactive. However, the DCV potential included 34.4-MeV deuteron scattering data from Newman *et al.* [47] for deuteron scattering off a number of neighboring nuclei.

The bound-state wave functions were calculated using a WS effective potential to bind the $\alpha$ particle to the deuteron in the entrance channel and to the target nucleus in the exit channel. The $\alpha$ + target bound-state geometry was parametrized by $R=1.25A_T^{1/3}$ fm and $a=0.65$ fm, with the depth of the potential wells independently adjusted to reproduce

TABLE I. Optical model parameters used in the DWBA calculations for $^6$Li scattering from $^{58}$Ni and $^{40}$Ca at $E(^6\text{Li})=34$ MeV. The parameters are defined in Eq. (5) with $W_D=0$ MeV and the radius convention $R_x=r_x A^{1/3}$ fm. The spin-orbit potential is $V_{LS}=3.0$ MeV, $r_{LS}=1.26$ fm, and $a_{LS}=0.65$ fm, while the Coulomb radius is $r_c=1.3$ fm.

| | Depth (MeV) | $r$ (fm) | $a$ (fm) |
|---|---|---|---|
| $^6$Li + $^{58}$Ni | | | |
| Real volume ($V_0$) | 112.49 | 1.324 | 0.825 |
| Imaginary volume ($W_i$) | 37.453 | 1.622 | 0.735 |
| $^6$Li + $^{40}$Ca | | | |
| Real volume ($V_0$) | 109.5 | 1.326 | 0.811 |
| Imaginary volume ($W_i$) | 46.24 | 1.534 | 0.884 |

the correct binding energy. The $\alpha$ + target wave functions were assumed to have six nodes for $^{62}$Zn ($^{44}$Ti) in the $0^+$ ground state and five nodes for $^{62}$Zn ($^{44}$Ti) in the $2^+$ first excited state. To describe the $\alpha+d$ bound state, we used the parametrization first suggested by Kubo and Hirata [48] with $R=1.9$ fm and $a=0.65$ fm for both the *S*-state and *D*-state wave functions with the potential depth independently adjusted for each. The *S*-state wave function included a single node while no nodes were included in the *D* state. Additionally, a Coulomb potential with radius $r_c=1.3$ fm was included in each bound state.

The DWBA calculations were performed using the computer code FRESCO [49]. The solid curves shown in Fig. 6 are the results of finite-range DWBA calculations including the parameters discussed above. It was found that the DWBA predictions for the cross section and $A_y$ had the same shape as the data but were out of phase by $\sim 6°$ for both the $^{58}$Ni($^6\vec{\text{Li}},d$)$^{62}$Zn and $^{40}$Ca($^6\vec{\text{Li}},d$)$^{44}$Ti reactions.

To improve the agreement between the DWBA calculations and the data, we made small changes in the OM and bound-state parameters to find the parameters which most affect the DWBA calculations. Small changes to the entrance channel $^6$Li OM parameters did not greatly affect the structure of the cross section and $A_y$ calculations, leaving the pattern of the angular distribution unchanged and producing only small variations in the amplitudes. The calculations were most sensitive to the radius parameters $r_0$ and $r_i$, however changes of up to $\pm 30\%$ did not greatly improve the agreement between the calculations and the data.

In the case of the exit channel deuteron OM parameters, the DWBA calculations were only sensitive to the real volume potential. It was found that a decrease of 12% in the radius parameter $r_0$ from 1.17 fm to 1.03 fm resulted in excellent agreement with the cross section and $A_y$ data for both the $^{58}$Ni($^6\vec{\text{Li}},d$)$^{62}$Zn and $^{40}$Ca($^6\vec{\text{Li}},d$)$^{44}$Ti reactions. A similar effect was noticed for a 16% decrease in the depth $V_0$. These decreases did alter the predictions of deuteron elastic scattering but were consistent at angles forward of 30° with the predictions without the change (i.e., using the unmodified DCV parameters). The dashed curves shown in Fig. 6 are the results of calculations performed with the deuteron OM radius parameter $r_0$ decreased to 1.03 fm. All further DWBA calculations were performed with this change.

Many factors affect the overall normalization of the calculated cross section, therefore we consider this quantity to have only limited usefulness. However, in light of the discussion in Sec. V we choose to report these normalizations. We define the normalization $S$ to be $(d\sigma/d\Omega)_{\text{exp}}=S(d\sigma/d\Omega)_{DW}$, where the DWBA cross section uses unit spectroscopic factor. Therefore, information on the spectroscopic factors for both the target and projectile are contained multiplied in $S$. For the $^{58}$Ni($^6\vec{\text{Li}},d$)$^{62}$Zn reaction, $S$ is equal to 2.5 and 0.75 for the g.s. and $2^+$ transition, respectively, while for the $^{40}$Ca($^6\vec{\text{Li}},d$)$^{44}$Ti reaction, $S$ is equal to 1.5 and 0.7 for the g.s. and $2^+$ transition, respectively. In all the figures, the one-step DWBA calculations of $d\sigma/d\Omega$ have been normalized by these factors.

During the analysis we found that it was necessary to have a deuteron spin-orbit potential in the exit channel in order to describe the transfer VAP data. We performed calculations with and without both the deuteron and $^6$Li spin-orbit potentials and found that the deuteron spin-orbit potential is necessary for generating $A_y$ in the ($^6$Li,$d$) reactions. This observation is in agreement with the work of Drummer *et al.* [39].

The overall very good agreement between the cross section and VAP data for the $^{40}$Ca and $^{58}$Ni reactions and the direct-transfer DWBA calculations is a strong indication that multistep processes are either weak for these transitions, or that they have the same overall form as the one-step process. Therefore, we proceed first with the one-step analysis of the TAP data for the determination of $\eta$, and then consider multistep processes in Sec. V.

### B. Determination of $\eta$

The *S*- and *D*-state wave functions were included in the calculations normalized by $b_0$ and $b_2$, respectively. The quantity $\eta$ is determined by taking the ratio of Eq. (1) for $l=2$ and $l=0$ and solving for $N_2/N_0$ as

$$\eta=\frac{N_2}{N_0}=\frac{b_2\,u_2(r)}{b_0\,u_0(r)}\,\frac{W_{-\xi,1/2}(2\beta r)}{W_{-\xi,5/2}(2\beta r)}. \tag{7}$$

For $r\gtrsim 5$ fm, which is when the approximation of Eq. (1) becomes valid, Eq. (7) becomes constant and $\eta$ can be reliably determined.

In determining the best fits to the TAP data, the value of $\eta$, as calculated by Eq. (7), was the only quantity allowed to vary, and the effects on the TAP were calculated with the first-order DWBA. As can be seen in Fig. 7 (and in Fig. 2 of Ref. [15]) the magnitude and sign of the TAPs $A_{zz}$ and $A_{xz}$ are sensitive to the magnitude and sign of $\eta$ included in the calculation. That is, the larger the value of $\eta$ included in the calculations, the larger the magnitude of the predicted TAP. Similarly, the signs of the predicted TAP (when not strongly oscillatory) tend to be opposite that of $\eta$. Therefore, a clear signature for $\eta$ is present in the predicted analyzing powers.

We have measured two TAPs for two different ($^6\vec{\text{Li}},d$) transfer reactions leading to two states in the final nuclei, giving us a total of eight TAP angular distributions. We determined the best value for $\eta$ for each of the eight TAPs by separately minimizing $\chi^2$, defined as

$$\chi^2=\sum_{i=1}^{N}\left[\frac{A_i^{\text{exp}}(\theta)-A_i^{\text{th}}(\theta)}{\Delta A_i^{\text{exp}}(\theta)}\right]^2, \tag{8}$$

for each TAP angular distribution. Here $A_i^{\text{exp}}$ and $\Delta A_i^{\text{exp}}$ are the experimental TAP data and associated errors, $A_i^{\text{th}}$ is the corresponding predicted TAP from the DWBA calculations, and the sum is over the number of data points $N$ for each TAP angular distribution.

The solid curves shown in Fig. 7 correspond to the best-fit $\eta$ values for each TAP. The eight values of $\eta$ determined in this way are summarized in Table II. The dashed and dotted curves correspond to calculations with $\eta=+0.015$ and $-0.015$, respectively.

The uncertainty in each of the eight determinations of $\eta$ results from a combination of statistical uncertainties and uncertainties in the DWBA parameters. The statistical uncertainty depends on the errors of the data points as well as the sensitivity of the calculation to changes in the value of $\eta$. This uncertainty was taken to be the difference between the value of $\eta$ for the minimum $\chi^2$ and the value for $\chi^2+1$. However, the $\chi^2$ per degree of freedom $\chi^2_\nu=\chi^2/(N-1)$ for six of the eight individual results was $>1$. At the same time, several of the calculations, particularly those for $A_{xz}$, were very sensitive to changes in $\eta$, resulting in smaller statistical uncertainties. Therefore, in order to more fairly weight those with poorer fits in the final analysis, we chose to multiply the statistical uncertainties of the six TAPs for which $\chi^2_\nu>1$, by the factor $\sqrt{\chi^2_\nu}$. The resulting uncertainties are denoted as $\Delta\eta_s$ and are summarized along with each $\chi^2_\nu$ in Table II.

The uncertainties in the DWBA parameters are more difficult to estimate. A systematic investigation of changes in the OM parameters showed that very few significantly affected the description of the cross section and VAPs for the ($^6$Li,$d$) reactions. Therefore, the OM parameters were held fixed to the best available parameters as described in Sec. IV A.

Next we checked the sensitivity of the DWBA calculations to the bound-state wave functions. The potential binding the $\alpha$ particle to the target nucleus has previously been set by a variety of criteria (see, for example, Refs. [42,50]). The calculated TAPs were influenced by the geometry of this potential. To reflect this sensitivity and to account for the differences in the geometry parameters found in the literature, we assigned them an overall uncertainty of $\pm 15\%$. Changes in the bound-state geometry by more than $\pm 15\%$ began to destroy the agreement between the calculations and the cross section and VAP data. The difference between the best-fit value of $\eta$ for the geometry parameters given above and the best-fit value of $\eta$ when each parameter was changed by $\pm 15\%$ was added in quadrature. The TAPs were found to be rather insensitive to the $d+\alpha$ bound-state geometry. Even an increase of $\sim 60\%$ in $R$ from 1.90 fm to 3.02 fm, which was the radius used in an analysis of the $^4$He($d,\gamma$)$^6$Li reaction [51], produced a change in the best-fit value of $\eta$ for each TAP which was less than the statistical uncertainty $\Delta\eta_s$ for each TAP. This effect was deemed minimal considering the large change in $R$. From this calculation, we find that the TAPs for ($^6\vec{\text{Li}},d$) reactions are, as expected, sensitive only to the tail of the bound-state $^6\text{Li}\rightarrow d+\alpha$ wave function.

TABLE II. Values of $\eta$ extracted for the pure one-step DWBA calculations from the TAP measurements of ($^6\vec{\text{Li}},d$) reactions. The uncertainties have been multiplied by $10^3$.

| Target | State | TAP | $\eta$ | $\chi^2_\nu$ | $\Delta\eta_s$ | $\Delta\eta_t$ |
|---|---|---|---|---|---|---|
| $^{58}$Ni | $0^+$ | $A_{zz}$ | $-0.0020$ | 3.39 | 3.7 | 4.5 |
| | | $A_{xz}$ | $+0.0021$ | 2.20 | 1.5 | 1.7 |
| | $2^+$ | $A_{zz}$ | $+0.0063$ | 1.63 | 2.6 | 9.0 |
| | | $A_{xz}$ | $-0.0007$ | 0.83 | 1.2 | 1.3 |
| $^{40}$Ca | $0^+$ | $A_{zz}$ | $+0.0024$ | 1.44 | 4.4 | 6.3 |
| | | $A_{xz}$ | $-0.0017$ | 2.80 | 5.4 | 7.9 |
| | $2^+$ | $A_{zz}$ | $+0.0114$ | 0.73 | 1.7 | 13.1 |
| | | $A_{xz}$ | $-0.0003$ | 5.53 | 2.6 | 2.9 |

Until now we have assumed that the TAPs for ($^6\vec{\text{Li}},d$) reactions are generated primarily by the $D$-state component in the $d+\alpha$ wave function. However, it has been shown that deuteron OM tensor potentials can affect the TAPs for deuteron-induced transfer reactions; see Refs. [4,5,52], for example. Therefore, we investigated whether deuteron or $^6$Li OM tensor potentials would affect the TAPs for the ($^6\vec{\text{Li}},d$) reactions. This was done by separately including deuteron and $^6$Li tensor potentials in the calculations and then determining if the best-fit value for $\eta$ changed. We used a deuteron-nucleus tensor potential adopted from the results of 30 MeV deuteron scattering from neighboring nuclei [53]. It was found that the TAPs were almost entirely insensitive to the deuteron tensor potential. The extracted values of $\eta$ changed by $\leqslant 0.0006$, with five of them by $\leqslant 0.0001$.

Very little systematic work has been done to establish the $^6$Li-nucleus tensor potential. To estimate its role in the present calculations we included the potential of Kerr *et al.* [38], which was derived from $^6\vec{\text{Li}}$ scattering on $^{12}$C at 30 MeV. The maximum change in $\eta$ due to the $^6$Li OM tensor potential was 0.0017 for one of the TAPs while six of the eight TAPs changed by $\leqslant 0.0010$. Therefore, it appears that neither a deuteron nor $^6$Li OM tensor potential affects the value of $\eta$ extracted in this work.

The uncertainty in each determination of $\eta$ was found by adding in quadrature the contributions from the statistical uncertainty, uncertainties due to the $\alpha$ + target bound state potential, and the deuteron and $^6$Li OM tensor potentials. This value is summarized in Table II as $\Delta\eta_t$. The final value of $\eta$ determined from an analysis of the TAPs from ($^6\vec{\text{Li}},d$) reactions was found by taking the average value of all eight determinations, weighted by the inverse square of the overall

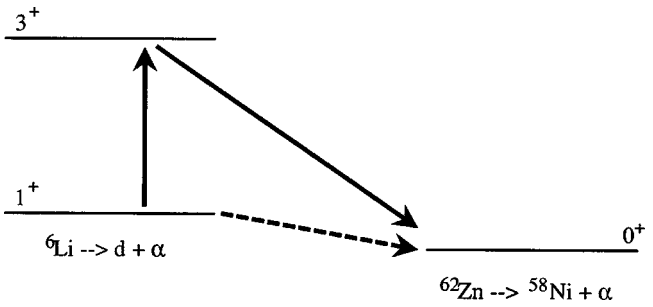


FIG. 8. Schematic of one- and two-step DWBA calculations. The dashed arrow represents a one-step $\alpha$ transfer while the solid arrows represent a two-step $\alpha$ transfer through the $3^+$ first-excited state in $^6$Li. For the case shown here, the transfers form the g.s. of $^{62}$Zn.

uncertainty $\Delta\eta_t$ for each determination, with the result being $\eta = +0.0003 \pm 0.0009$.

## V. HIGHER-ORDER PROCESSES

In the analysis we have presented so far the procedure for the determination of $\eta$ from a study of $(^6\vec{\text{Li}},d)$ reactions assumes a direct $\alpha$-particle transfer mechanism. The question can be raised as to the possible effects of more complicated transfer reaction mechanisms, such as higher-order couplings via other intermediate states, on the conclusions reached in the previous section and in Ref. [15]. In the discussions in this section our goal is to identify the influence of two-step mechanisms in the analysis, and to investigate the role the two-step processes play in the current determination of the $\eta$ parameter.

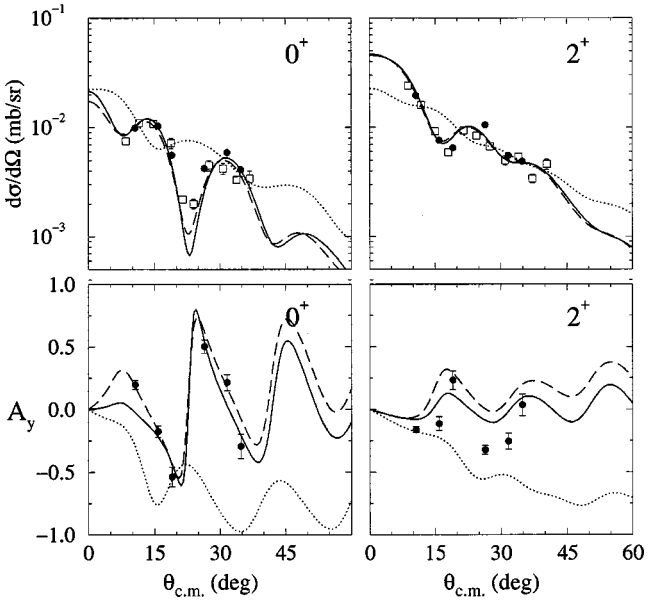


FIG. 9. Angular distributions of $d\sigma/d\Omega$ and $A_y$ for the $^{58}$Ni$(^6\vec{\text{Li}},d)^{62}$Zn reaction at $E(^6\text{Li}) = 34$ MeV leading to the $0^+$ g.s. and the $2^+$ first excited state. The open squares (□) are from Ref. [41] while the closed circles (●) are the present data. The solid curves are the results of one-step DWBA calculations. The dotted (dashed) curves are combined one- and two-step calculations, where the two-step calculation goes only through the $3^+$ state, with the two-step amplitude equal to 1.0 (0.27). The calculations of $d\sigma/d\Omega$ are normalized to the data.

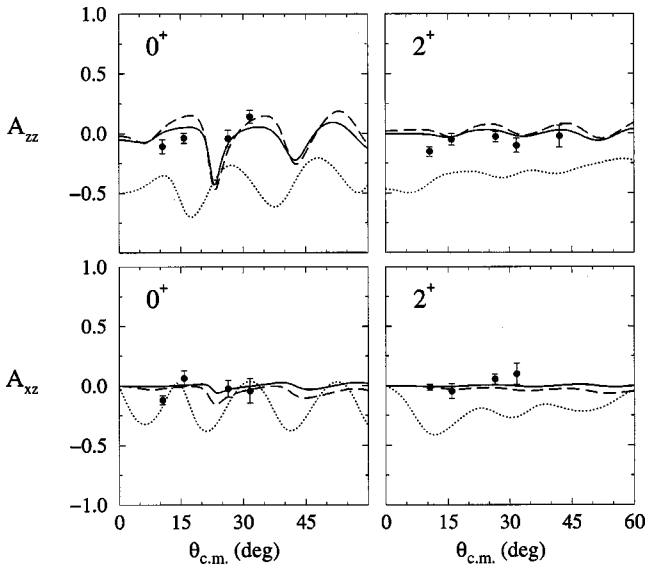


FIG. 10. Angular distributions of $A_{zz}$ and $A_{xz}$ for the $^{58}$Ni$(^6\vec{\text{Li}},d)^{62}$Zn reaction at $E(^6\text{Li}) = 34$ MeV leading to the $0^+$ g.s. and the $2^+$ first excited state. The curves are the same as in Fig. 9. For all calculations $\eta = 0$.

There are many kinds of couplings that should be distinguished. The first are the coupled channels processes which affect elastic scattering. These are, or should be, included effectively in the optical model potentials, regardless of the complicated mechanism of excitations that may cause them. As discussed in Sec IV A, we obtained good agreement between the elastic scattering data and the OMP calculations (see Fig. 4). It is therefore reasonable to assume that channel couplings between the ground and excited states are implicitly accounted for in the OMP. The second kind of couplings that may be present are the two-step or multistep reaction mechanisms that affect specific reaction channels, and cannot be taken into account by the optical potentials. We will therefore focus in this section on two-step processes which, due to the cluster structure of the projectile, are most likely to affect the analysis of transfer reaction observables. We neglect however excitations of the target and of the final nucleus, as well as all types of multistep processes involving the target and the projectile simultaneously.

### A. Two-step couplings

To investigate the effects of the $^6$Li excited states we describe them in a combined first- and second-order DWBA calculation, where we supplement the direct process with two-step transitions in which the $^6$Li is first excited to one of the three low-lying $T=0$ excited states ($J^\pi = 3^+$, $E_x = 2.19$ MeV; $J^\pi = 2^+$, $E_x = 4.31$ MeV; $J^\pi = 1^+$, $E_x = 5.65$ MeV) followed by the $\alpha$ particle transfer to the tar-

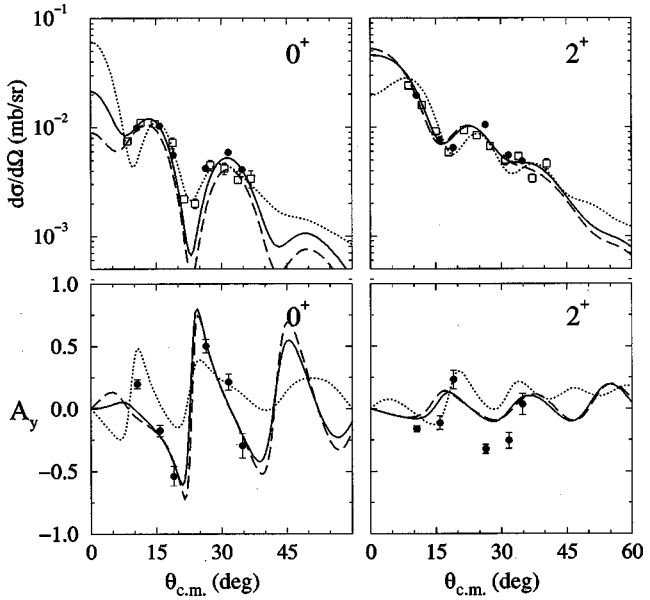


FIG. 11. Angular distributions of $d\sigma/d\Omega$ and $A_y$ for the $^{58}$Ni($^{6}\vec{\text{Li}}$,$d$)$^{62}$Zn reaction at $E(^6\text{Li})=34$ MeV leading to the $0^+$ g.s. and the $2^+$ first excited state. The solid curves are the pure one-step DWBA calculations as in Fig. 9. The dotted (dashed) curves correspond to combined one- and two-step DWBA calculations, where the two-step goes through all three excited states ($3^+$, $2^+$, and $1^+$), with the two-step amplitudes equal to 1.0 (0.27). The calculations of $d\sigma/d\Omega$ are normalized to the data.

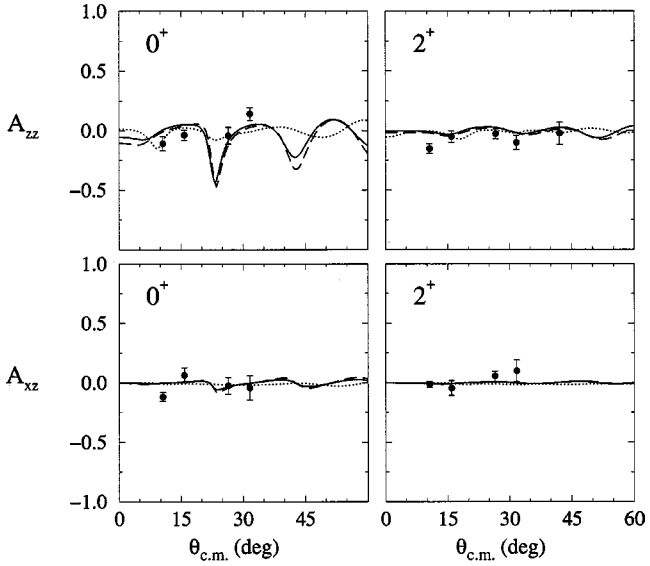


FIG. 12. Angular distributions of $A_{zz}$ and $A_{xz}$ for the $^{58}$Ni($^{6}\vec{\text{Li}}$,$d$)$^{62}$Zn reaction at $E(^6\text{Li})=34$ MeV leading to the $0^+$ g.s. and the $2^+$ first excited state. The curves are the same as in Fig. 11. For all calculations $\eta=0$.

get nucleus. For the purposes of this discussion we confine ourselves to an analysis of the $^{58}$Ni($^{6}\vec{\text{Li}}$,$d$)$^{62}$Zn reaction.

In the first two-step DWBA calculations we assume that the reaction proceeds via the lowest excited state ($J^\pi=3^+$), as shown schematically in Fig. 8. We neglect the explicit couplings back to the elastic channel, since the elastic optical potential is assumed to be accurate. This state played a crucial role in the analysis of the ($d$,$^6$Li) reaction investigated in Ref. [35]. The wave function for the unbound $3^+$ state in $^6$Li was assumed to have $l=2$ and was obtained using the same potential geometry as that used to generate the g.s. wave functions. The potential depth was adjusted using the weak binding energy approximation [20], in order to describe the $d+\alpha$ wave function by that of a slightly bound state. The free parameter in the two-step calculations is the spectroscopic amplitude $A$, which initially is expected to be equal to unity on the basis of a pure $d+\alpha$ cluster model for the excited states of $^6$Li.

Comparison of one-step DWBA calculations with combined one- and two-step calculations is shown in Fig. 9. Calculations with $A=1.0$ are out of phase with the cross-section data and the calculated VAPs are negative whereas the data are oscillatory about zero. Furthermore, the shape of the angular dependence of these two observables is substantially different from the data. We obtained however a good agreement between the combined calculations and the data when $A$ was decreased from 1.0 to 0.27. These results are close to the one-step calculations and provide better agreement with the forward angle VAP data for the g.s. transition. It is worth noting that for $A=0.27$ the cross-section normalization factor $S$ is equal to 3.0 and 0.85 for the g.s. and $2^+$ transitions, respectively, while for $A=1.0$ $S$ is equal to 1.0 and 0.2 for the same transitions since the two-step routes enhance the predicted magnitudes of the cross sections.

It is interesting to note that the magnitude of the predicted VAP is larger when $A=1.0$, and that similar enhancements were found by Bowsher *et al.* [35] for the VAP in the $^{64}$Zn($\vec{d}$,$^6$Li)$^{60}$Ni reaction. From a simple model they predicted that the $3^+$ state would generate negative VAPs, similar to their VAP data. Thus they concluded that the $3^+$ state plays an important role in the reaction at $E_d=16.4$ MeV. Our calculations indicate that at the reaction energy of the present study the $3^+$ state might be relatively less important.

In Fig. 10 we show the same calculations for the TAPs $A_{zz}$ and $A_{xz}$. At this stage the calculations do not include a $D$ state in the $^6$Li g.s. wave function, i.e., $\eta=0$. We see that the calculations with $A=1.0$ predict relatively large TAPs compared to both the data and one-step calculations while the calculations with $A=0.27$ resemble quite closely the one-step calculations for both TAPs.

In order to improve the two-step description, we performed calculations which, in addition to the $3^+$ state, also include the $2^+$ and the $1^+$ states. We assume that these three states form a spin multiplet and we describe them by similar spatial wave functions and in the DWBA calculations we use the same amplitude $A$ for each state. In Fig. 11 we show a comparison of the one-step calculations with combined calculations allowing transfer through the three excited states. When $A=1.0$ (dotted curves), we see that the agreement with the cross section and VAP data is worse than that for the one-step calculations. In this case the normalization factor $S$ is equal to 0.25 and 0.08 for the g.s. and $2^+$ transitions, respectively. If $A=0.27$ (dashed curves), we find that the

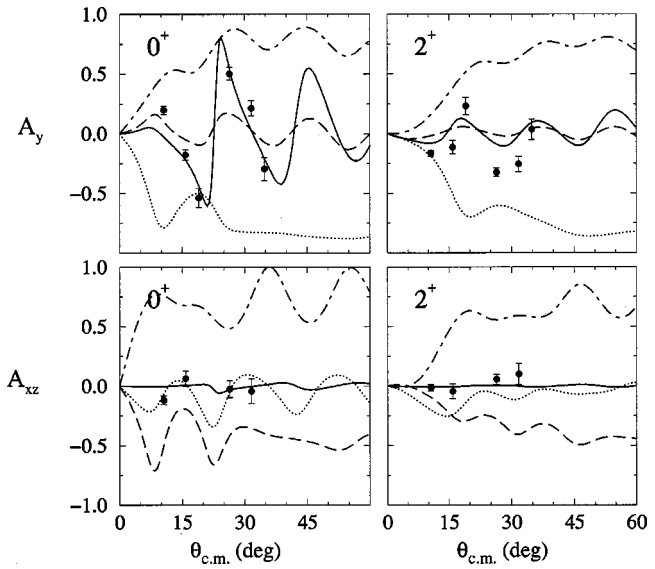


FIG. 13. Angular distributions of $A_y$ and $A_{xz}$ for the $^{58}$Ni($^6\vec{\text{Li}},d$)$^{62}$Zn reaction at $E(^6\text{Li})=34$ MeV leading to the $0^+$ and $2^+$ states. The dotted, dashed, and dot-dashed curves correspond to pure two-step DWBA calculations, through only the $3^+$ state, only the $2^+$ state, and only the $1^+$ state, respectively, with unit amplitude and $\eta=0$. The solid line represents the one-step DWBA prediction.

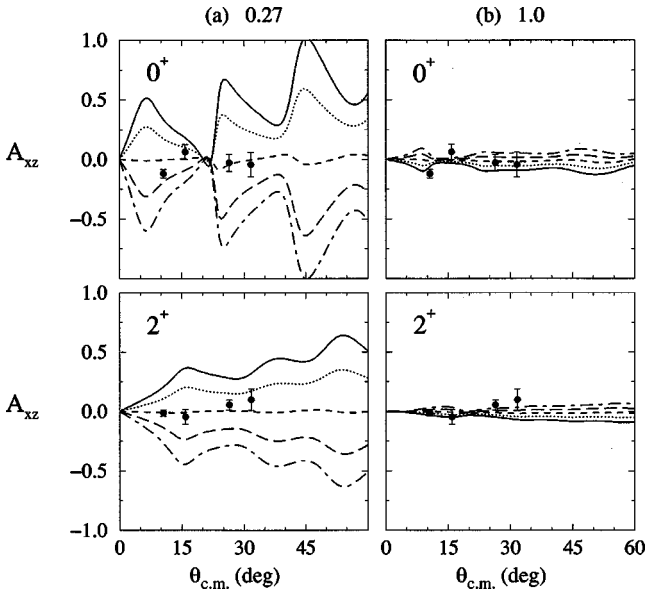


FIG. 14. Effects of variation of $\eta$ on the angular distributions of $A_{xz}$ for the $^{58}$Ni($^6\vec{\text{Li}},d$)$^{62}$Zn reaction at $E(^6\text{Li})=34$ MeV leading to the $0^+$ and the $2^+$ states, from combined one- and two-step DWBA calculations through all excited states, with two-step amplitudes of (a) 0.27 and (b) 1.0. The solid, dotted, short-dashed, long-dashed, and dot-dashed curves correspond to calculations with $\eta=-0.0112$, $-0.0056$, 0, $+0.0056$, and $+0.0112$, respectively.

agreement with the data is very good, with almost no change in the predictions from the one-step calculations. We found that calculations with either amplitude resulted in very small predicted TAPs, as shown in Fig. 12. We have used other intermediate amplitudes $0.4\leqslant A\leqslant 0.8$ and we found that, although there was some change in the predicted cross section and VAP, the predicted TAPs were always nearly zero.

It is important to emphasize that no matter what amplitude we choose for the two-step component, provided that we include all three excited states with equal amplitudes, the TAPs are not significantly changed from the predictions of the one-step calculation. The fact that the three excited states are part of a spin multiplet justifies the use of a common value, which is predicted to be unity in a pure $d+\alpha$ model of $^6$Li. However there are no strong theoretical reasons to use any specific value for *A*. Fixing these individual amplitudes experimentally would require measuring the breakup processes which populate those $^6$Li resonant states or performing an experiment in inverse kinematics which measured the $^6$Li($^{58}$Ni,$^{58}$Ni)$^6$Li$^\star$ cross sections.

To understand the mechanism of the cancellation in the TAPs that arises when we include all three states, we performed calculations where we turned off the one-step mechanism and considered pure two-step transfers via each of the individual states. Figure 13 shows the predicted analyzing powers for the different pure two-step transfers. The calculated analyzing powers behave quite differently for the three cases. The predicted analyzing powers are large and of opposite sign for the $3^+$ and $1^+$ transfers, and are generally much smaller for the $2^+$ transfer. It is interesting to note that this feature has already been observed in the work of Ref. [35] when transitions of the $\alpha$ particle to *D*-wave $J^\pi=3^+$, $2^+$, and $1^+$ $^6$Li states were considered. If we interpret these states as $d+\alpha$ clusters with angular momentum *l* and assume that the spin of the deuteron *s* produces the spin of the $^6$Li nucleus, the $3^+$ state acts as a spin filter as it tends to align $\vec{l}$ and $\vec{s}$. On the contrary, when we include all three states this preference is lost by the mixing of a nonaligned state $(2^+)$ and an antialigned state $(1^+)$.

### B. Determination of $\eta$

If we allow all three excited states each with $A=0.27$ to contribute to the reaction, we find that the combined calculations (dashed curves in Figs. 11 and 12) resemble quite closely the one-step calculations for all observables. Furthermore, when the sensitivity of the TAPs to $\eta$ was investigated we found that the TAPs behaved the same way as for one-step calculations. Larger values of $\eta$ generated larger predicted TAPs, particularly for $A_{xz}$, as shown in Fig. 14(a). The best-fit value for $\eta$, weighted by the uncertainty $\Delta\eta_s$ is $\eta=0.0003$.

When we investigated the sensitivity to $\eta$ when $A=1.0$, we found an interesting feature. The calculations showed much less sensitivity to changes in $\eta$ than before, as we can see in the $A_{xz}$ results of Fig. 14(b). Furthermore, the sign of the predicted TAPs tended to have the same sign as $\eta$, opposite to the findings of our previous one-step analysis. For changes in $\eta$ of between $-0.011$ to $+0.011$ the predicted magnitudes for $A_{zz}$ were typically $\lesssim 0.2$ while the predicted

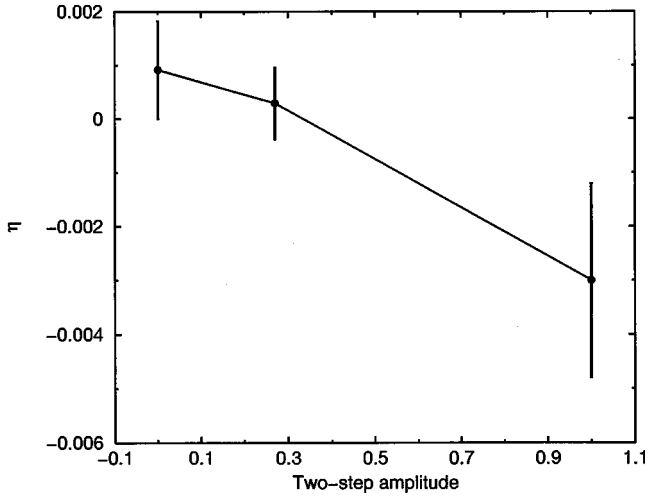


FIG. 15. Effects on the extracted $\eta$ value of various amplitudes of two-step mechanisms, from analysis of $A_{zz}$ and $A_{xz}$ for the $^{58}$Ni($^{6}\vec{\text{Li}},d$)$^{62}$Zn reaction at $E(^{6}\text{Li})=34$ MeV leading to the $0^{+}$ g.s. and the $2^{+}$ first excited state.

magnitudes for $A_{xz}$ were typically $\lesssim 0.1$. We determined in this case, which has slightly poorer agreement with the cross section and $A_y$ data, the best-fit value of $\eta=-0.0030$. With $A=1.0$ the reaction is more likely to proceed through the two-step channel as evidenced by the cross-section normalizations $S$, and therefore the sensitivity to the details of the ground-state wave function is diminished since the $\alpha$ particle is more likely transferred from the excited states and not from the $D$ state in the ground state.

If we average the best values for $\eta$ weighted only by their uncertainties $\Delta\eta_s$ from our results of the combined calculations with $A=1.0$, we find $\eta=-0.0030\pm0.0022$, while for the combined calculations with $A=0.27$, we find $\eta=+0.0003\pm0.0006$. In order to more fairly compare our combined one- and two-step results with our previous pure one-step result, we must reduce the data set used to calculate the pure one-step result. If we average similarly the best value for $\eta$ from the one-step calculations using only the $^{58}$Ni($^{6}\vec{\text{Li}},d$)$^{62}$Zn data weighted by the uncertainty $\Delta\eta_s$ and compare this result with the results from the combined calculations, we find that the magnitude of the extracted $\eta$ is increasing with increasing $A$, as shown in Fig. 15. The value of $\eta$ becomes increasingly more negative as more two-step processes are included, with an increased error bar when $A=1.0$. However even with a large contribution from the two-step mechanisms, as long as the amplitudes $A$ are equal, the extracted $\eta$ value remains very close to zero.

## VI. DISCUSSION AND CONCLUSIONS

We have measured the analyzing powers $A_y$, $A_{zz}$, and $A_{xz}$ for the $^{58}$Ni($^{6}\vec{\text{Li}},d$)$^{62}$Zn and $^{40}$Ca($^{6}\vec{\text{Li}},d$)$^{44}$Ti reactions leading to the ground and first excited state for each at $E(^{6}\text{Li})=34$ MeV. These data represent the first analyzing power measurements for ($^{6}\vec{\text{Li}},d$) reactions on any target heavier than $^{12}$C. Additionally, we have measured the relative cross section for the $^{58}$Ni($^{6}$Li,$d$)$^{62}$Zn reaction and the cross section and VAP for $^{6}\vec{\text{Li}}+^{58}$Ni scattering, also at 34 MeV.

The reaction data have been included in a direct $\alpha$-transfer DWBA analysis. Very good agreement is achieved with the cross section and VAP data. We determined the asymptotic $D/S$ ratio $\eta$ for the $d+\alpha$ relative wave function in $^{6}$Li from an analysis of the TAP data. It was found that the TAPs were sensitive to the details of the $\alpha$ + target bound-state geometry and insensitive to the $\alpha+d$ bound-state geometry. Furthermore, OM tensor potentials had very little effect on the calculated ($^{6}\vec{\text{Li}},d$) TAPs. Fitting the eight TAP angular distributions individually, and taking into account uncertainties in the data and input model parameters, we find a value of $\eta=+0.0003\pm0.0009$.

We performed an investigation of the effects of two-step reaction mechanisms on the present data. Allowing only the $J^{\pi}=3^{+}$ state to contribute to the two-step mechanism, we must reduce the amplitude of the two-step component to 0.27 in order to maintain agreement with the cross section and VAP data. Allowing the $J^{\pi}=3^{+}$, $2^{+}$, and $1^{+}$ states to contribute with the same amplitude to the two-step mechanism we achieve a reasonable agreement with the cross section and VAP data, even when the amplitude of the two-step component is not reduced and the reaction is dominated by the two-step component. For the reduced amplitude of the two-step component, the results for the cross section and VAP observables are almost unchanged compared with the one-step results. The predictions for the TAP, however, are not significantly changed for any reasonable amplitude we choose for the two-step mechanism. For unit two-step amplitudes, a best-fit value of $\eta=-0.0030\pm0.0022$ was determined. Though this is slightly larger in magnitude than our previous one-step result, it strengthens our conclusion that $\eta$ is very small, much smaller than most theoretical and experimental studies.

The cumulative results obtained both by theoretical and experimental methods point predominantly to a negative value of $\eta$ (see Fig. 1), but the magnitude is still not clearly determined. The published [25] and improved [26] VMC results are likely to be overestimated, as they lead to a quadrupole moment far too large if compared with the experimental value (about a factor of 10 for the first one and a factor of 4 for the second), and they also predict tensor observables far too large [33] compared to the data. In order to reproduce the experimental value of $Q$, if we accept some kind of correlation between $\eta$ and $Q$ similar to what has been found in the various theoretical models, we would have to obtain an experimental determination for $\eta$ about four times smaller in magnitude than the Wiringa value [26]. This further suggests that the recent [32] experimental determination of $\eta$, compatible with the latest VMC theoretical prediction, may also be overestimated.

Our present determination provides evidence that the $D$ state in $^{6}$Li associated with the $d+\alpha$ component of the wave function is extremely small and indicates a need for further theoretical investigation. Hopefully this will enable us to understand the connections between the different $D$-state observables in $^{6}$Li, probably through some more

complicated exchange mechanisms still absent from many of the present models.

## ACKNOWLEDGMENTS

We would like to thank P. V. Green, P. L. Kerr, A. J. Mendez, E. G. Myers, and B. G. Schmidt for their assistance with the experiments, and Z. Ayer for contributions in the early stages of this project. This work was supported in part by the U.S. DOE under Grant No. DE-FG02-97ER41041, the NSF under Grant. No. NSF-PHY-95-23974, the Portuguese FCT under Contract Praxis/2/2.1/FIS/223/94, the Polish KBN under Grant No. 2 P03B 056 12, and the British EPSRC under Grant No. GR/L/94574.

[1] A.M. Eiró and F.D. Santos, J. Phys. G **16**, 1139 (1990).
[2] N.R. Rodning and L.D. Knutson, Phys. Rev. C **41**, 898 (1990).
[3] D.R. Lehman, Colloq. Phys. Suppl. n22,, **51**, C6-47 (1990), and references therein.
[4] B. Kozlowska, Z. Ayer, R.K. Das, H.J. Karwowski, and E.J. Ludwig, Phys. Rev. C **50**, 2695 (1994).
[5] Z. Ayer, H.J. Karwowski, B. Kozlowska, and E.J. Ludwig, Phys. Rev. C **52**, 2851 (1995).
[6] J.L. Friar, B.F. Gibson, D.R. Lehman, and G.L. Payne, Phys. Rev. C **37**, 2859 (1988).
[7] Y. Wu, S. Ishikawa, and T. Sasakawa, Few-Body Syst. **15**, 145 (1993).
[8] A. Kievsky, S. Rosati, M. Viviani, C.R. Brune, H.J. Karwowski, E.J. Ludwig, and M.H. Wood, Phys. Lett. B **406**, 292 (1997).
[9] B.C. Karp, E.J. Ludwig, J.E. Bowsher, B.L. Burks, T.B. Clegg, F.D. Santos, and A.M. Eiró, Nucl. Phys. **A457**, 15 (1986).
[10] E.R. Crosson, S.K. Lemieux, E.J. Ludwig, W.J. Thompson, M. Bisenberger, R. Hertenberger, D. Hofer, H. Kader, P. Schiemenz, G. Graw, A.M. Eiró, and F.D. Santos, Phys. Rev. C **47**, 2690 (1993).
[11] H.R. Weller and D.R. Lehman, Annu. Rev. Nucl. Sci. **38**, 563 (1988).
[12] D. Albrecht, M. Csatlos, J. Ero, Z. Fodor, I. Hernyes, Mu Hongsung, B.A. Khomenko, N.N. Khovanskij, P. Koncz, Z.V. Krumstein, Y.P. Merekov, V.I. Petrukhin, Z. Seres, and L. Vegh, Nucl. Phys. **A338**, 477 (1980).
[13] R. Ent, H.P. Block, J.F.A. van Hienen, G. van der Steenhoven, J.F.J. van den Brand, J.W.A. den Herder, E. Jans, P.H.M. Keizer, L. Lapikas, E.N.M. Quint, P.K.A. de Witt Huberts, B.L. Berman, W.J. Brisco, C.T. Christou, D.R. Lehman, N.E. Norum, and A. Saha, Phys. Rev. Lett. **57**, 2367 (1986).
[14] N.W. Schellingerhout, L.P. Kok, S.A. Coon, and R.M. Adam, Phys. Rev. C **48**, 2714 (1993); **52**, 439 (1995).
[15] K.D. Veal, C.R. Brune, W.H. Geist, H.J. Karwowski, E.J. Ludwig, A.J. Mendez, E.E. Bartosz, P.D. Cathers, T.L. Drummer, K.W. Kemper, A.M. Eiró, F.D. Santos, B. Kozlowska, H.J. Maier, and I.J. Thompson, Phys. Rev. Lett. **81**, 1187 (1998).
[16] K.D. Veal, Ph.D. thesis, University of North Carolina at Chapel Hill, 1998.
[17] K. Varga and R.G. Lovas, Phys. Rev. C **43**, 1201 (1991), and references therein.
[18] D. Sunhdolm, P. Pyykkö, L. Laaksonen, and A.J. Sadlej, Chem. Phys. Lett. **112**, 1 (1984).
[19] H. Nishioka, J.A. Tostevin, R.C. Johnson, and K.-I. Kubo, Nucl. Phys. **A415**, 230 (1984); H. Nishioka, J.A. Tostevin, and R.C. Johnson, Phys. Lett. **124B**, 17 (1983).
[20] P.R. Dee, C.O. Blyth, H.D. Choi, N.M. Clarke, S.J. Hall, O. Karban, I. Martel-Bravo, S. Roman, G. Tungate, R.P. Ward, N.J. Davis, D.B. Steski, K.A. Connell, and K. Rusek, Phys. Rev. C **51**, 1356 (1995).
[21] V.I. Kukulin, V.N. Pomerantsev, K.D. Razikov, V.T. Voronchev, and G.G. Ryzhikh, Nucl. Phys. **A586**, 151 (1995).
[22] P. Navrátil and B.R. Barrett, Phys. Rev. C **54**, 2986 (1996).
[23] B.S. Pudliner, V.R. Pandharipande, J. Carlson, and R.B. Wiringa, Phys. Rev. Lett. **74**, 4396 (1995).
[24] B.S. Pudliner, V.R. Pandharipande, J. Carlson, S.C. Pieper, and R.B. Wiringa, Phys. Rev. C **56**, 1720 (1997).
[25] J.L. Forest, V.R. Pandharipande, S.C. Pieper, R.B. Wiringa, R. Schiavilla, and A. Arriaga, Phys. Rev. C **54**, 646 (1996).
[26] R.B. Wiringa (private communication).
[27] M.P. Bornand, G.R. Plattner, R.D. Viollier, and K. Alder, Nucl. Phys. **A294**, 492 (1978).
[28] K. Rusek, N.M. Clarke, G. Tungate, and R.P. Ward, Phys. Rev. C **52**, 2614 (1995).
[29] V. Punjabi, C.F. Perdrisat, E. Cheung, J. Yonnet, M. Boivin, E. Tomasi-Gustafsson, R. Siebert, R. Frascaria, E. Warde, S. Belostotsky, O. Miklucho, V. Sulimov, R. Abegg, and D.R. Lehman, Phys. Rev. C **46**, 984 (1992).
[30] F.D. Santos, I.J. Thompson, and A.M. Eiró, Colloq. Phys., Suppl. n22, **51**, C6-443 (1990).
[31] V.I. Kukulin, V.N. Pomerantsev, S.G. Cooper, and S.B. Dubovichenko, Phys. Rev. C **57**, 2462 (1998).
[32] E.A. George and L.D. Knutson, Phys. Rev. C **59**, 598 (1999).
[33] A.M. Eiró and I.J. Thompson, Phys. Rev. C **59**, 2670 (1999).
[34] E.A. George and L.D. Knutson, Phys. Rev. C **48**, 688 (1993).
[35] J.E. Bowsher, T.B. Clegg, H.J. Karwowski, E.J. Ludwig, W.J. Thompson, and J.A. Tostevin, Phys. Rev. C **45**, 2824 (1992).
[36] E. G. Myers, A. J. Mendez, B. G. Schmidt, and K. W. Kemper, Nucl. Instrum. Methods Phys. Res. B **56/57**, 1156 (1991).
[37] A.J. Mendez, E.G. Myers, K.W. Kemper, P.L. Kerr, E.L. Reber, and B.G. Schmidt, Nucl. Instrum. Methods Phys. Res. A **329**, 37 (1993).
[38] P.L. Kerr, K.W. Kemper, P.V. Green, K. Mohajeri, E.G. Myers, D. Robson, and B.G. Schmidt, Phys. Rev. C **52**, 1924 (1995).
[39] T.L. Drummer, E.E. Bartosz, P.D. Cathers, M. Fauerbach, K.W. Kemper, E.G. Myers, and K. Rusek, Phys. Rev. C **59**, 2574 (1999).
[40] R.I. Cutler, M.J. Nadworny, and K.W. Kemper, Phys. Rev. C **15**, 1318 (1977).
[41] R.R. Betts, N. Stein, J.W. Sunier, and C.W. Woods, Phys. Lett. **76B**, 47 (1978).
[42] H.W. Fulbright, C.L. Bennett, R.A. Lindgren, R.G. Markham, S.C. McGuire, G.C. Morrison, U. Strohbusch, and J. Tōke, Nucl. Phys. **A284**, 329 (1977).

[43] J. Cook, Nucl. Phys. **A388**, 153 (1982).
[44] J. Cook, Comput. Phys. Commun. **31**, 363 (1984).
[45] L.T. Chua, F.D. Becchetti, J. Jänecke, and F.L. Milder, Nucl. Phys. **A273**, 243 (1976).
[46] W.W. Daehnick, J.D. Childs, and Z. Vrcelj, Phys. Rev. C **21**, 2253 (1980).
[47] E. Newman, L.C. Becker, B.M. Preedom, and J.C. Hiebert, Nucl. Phys. **A100**, 225 (1967).
[48] K.-I. Kubo and M. Hirata, Nucl. Phys. **A187**, 186 (1972).
[49] I.J. Thompson, Comput. Phys. Rep. **7**, 167 (1988).
[50] A. Vitturi, L. Ferreira, P.D. Kunz, H.M. Sofia, P.F. Bortignon, and R.A. Broglia, Nucl. Phys. **A340**, 183 (1980); J. Cook, *ibid.* **A417**, 477 (1984); K. Umeda, T. Yamaya, T. Suehiro, K. Takimoto, R. Wada, E. Takada, S. Shimoura, A. Sakaguchi, S. Murakami, M. Fukada, and Y. Okuma, *ibid.* **A429**, 88 (1984).
[51] R. Crespo, A.M. Eiró, and F.D. Santos, Phys. Rev. C **39**, 305 (1989).
[52] O. Karban and J.A. Tostevin, Phys. Lett. **103B**, 259 (1981).
[53] G. Perrin, Nguyen Van Sen, J. Arvieux, R. Darves-Blanc, J.L. Durand, A. Fiore, J.C. Gondrand, F. Merchez, and C. Perrin, Nucl. Phys. **A282**, 221 (1977).